Heliyon 10 (2024) e31462

Contents lists available at ScienceDirect

Heliyon

journal homepage: www.cell.com/heliyon

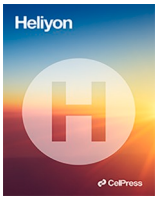

Research article

Aluminum oxide, cobalt aluminum oxide, and aluminum-doped zinc oxide nanoparticles as an effective antimicrobial agent against pathogens

Mohamad Omeiri [a,*], Esraa El Hadidi [b], Ramadan Awad [c,d], Jamalat Al Boukhari [c], Hoda Yusef [e]

[a] Department of Biology, Faculty of Arts and Sciences, University of Balamand, Beirut, Lebanon
[b] Department of Biological Sciences, Faculty of Science, Beirut Arab University, Beirut, Lebanon
[c] Department of Physics, Faculty of Science, Beirut Arab University, Beirut, Lebanon
[d] Department of Physics, Faculty of Science, Alexandria University, Alexandria, Egypt
[e] Department of Botany and Microbiology, Faculty of Science, Alexandria University, Alexandria, Egypt

ARTICLE INFO

Keywords:
Aluminum oxide
Cobalt aluminum oxide
Aluminum doped zinc oxide
Nanoparticles
Antimicrobial activity
Time-kill assay

ABSTRACT

Since the clock of antimicrobial resistance was set, modern medicine has shed light on a new cornerstone in technology to overcome the worldwide dread of the post-antimicrobial era. Research organizations are exploring the use of nanotechnology to modify metallic crystals from macro to nanoscale size, demonstrating significant interest in the field of antimicrobials. Herein, the antimicrobial activities of aluminum oxide (Al_2O_3), cobalt aluminum oxide ($CoAl_2O_4$), and aluminum doped zinc oxide ($Zn_{0.9}Al_{0.1}O$) nanoparticles were examined against some nosocomial pathogens. The study confirmed the formation and characterization of Al_2O_3, $CoAl_2O_4$, and $Zn_{0.9}Al_{0.1}O$ nanoparticles using various techniques, revealing the generation of pure nanoscale nanoparticles. With inhibition zones ranging from 9 to 14 mm and minimum inhibitory concentrations varying from 4 mg/mL to 16 mg/mL, the produced nanoparticles showed strong antibacterial activity against *Escherichia coli*, *Klebsiella pneumoniae*, *Pseudomonas aeruginosa*, and *Staphylococcus aureus*. Meanwhile, the bactericidal concentrations ranged from 8 mg/mL to 40 mg/mL. In culture, $Zn_{0.9}Al_{0.1}O$ NPs demonstrated a unique ability to inhibit the development of nosocomial infections with high bactericidal activity (8 mg/mL). Transmission electron microscope images revealed changes in cell shape, bacterial cell wall morphology, cytoplasmic membrane, and protoplasm due to the introduction of tested nanoparticles. These results pave the way for the use of these easily bacterial wall-piercing nanoparticles in combination with potent antibiotics to overcome the majority of bacterial strains' resistance.

1. Introduction

Disinfectants are the first line of defense that acts as a protective barrier against most types of infections. Despite recent advancements in the field of hygiene in industries, restaurants, schools, and hospitals, disinfection is considered one of the most critical public health concerns globally. Above all, infectious microorganisms pose significant health risks due to the emergence of over 300

* Corresponding author.
E-mail address: Mohamad.omeiri@fty.balamand.edu.lb (M. Omeiri).

https://doi.org/10.1016/j.heliyon.2024.e31462
Received 13 May 2024; Received in revised form 15 May 2024; Accepted 16 May 2024
Available online 16 May 2024

new infectious diseases [1,2]. To combat this, numerous disinfection techniques have been utilized to minimize infections by killing or inhibiting microorganisms. Miscellaneous compounds have been efficiently employed to protect facilities from microorganisms, including alcohol, aldehydes, quaternary ammonium cations, and some other oxidizing agents like hydrogen peroxide. Although such disinfectants are efficient, less expensive, plentiful in number, and do not produce hazardous substances after application, they have a number of limitations, including toxicity, bacterial resistance, and corrosiveness [3].

To address these limitations, nanoparticles were considered the "golden ticket" that moved disinfectants to higher levels. According to the International Organization for Standardization, a nanomaterial is defined as a material with an external size of 1–100 nm that has also been in the multi-fold domain owing to its notable features. By optimizing their physicochemical characteristics, different nanomaterials have been used as effective disinfectants [4,5]. As a result, numerous researchers are working to develop multifunctional nanomaterials that may be used as powerful disinfectants in different fields, among them medical devices, food preservatives, hospital-acquired disinfectants, and water disinfectants, among others [6]. The popularity of nano-based materials as an antimicrobial agent is due to the fact that their minute size and high surface-to-volume ratio result in greater surface exposure to germs, resulting in improved antimicrobial activity, which originates from the fact that such materials can use their reactive oxygen species to damage microorganisms or bind to their DNA or RNA, limiting their reproductive process [7,8].

Aluminum oxide, often known as alumina, is a white oxide. Alumina is a broad term for corundum-like formations in which oxygen atoms are packed hexagonally close together and alumina atoms occupy two-thirds of the octahedral positions in the lattice [9]. Alumina exists in numerous phases, including gamma, delta, theta, and alpha. The α alumina phase, on the other hand, is the most thermodynamically stable. Alumina has numerous fascinating features in general, such as high hardness, high stability, high insulation, and transparency [10]. Metal oxide materials are plentiful, with aluminum oxide nanostructure being the top-listed one that finds extensive use in a variety of industrial applications [11–13].

Cobalt and aluminum oxides combine to form the binary oxide known as cobalt aluminate, which is a stable chemical with a blue pigment known for its uses in glass, rubber, and plastics, among others [14]. Its distinctive optical characteristics cause it to be widely used in microelectronics [15,16]. Nonetheless, cobalt nanoparticles are involved in different biomedical applications based on their magnetic characteristics, such as site-specific medication delivery for cancer treatments and contrast enhancement agents for magnetic resonance imaging [17–19].

Zinc oxide ZnO, an inorganic conductor and II-IV semiconductor, has a high exciton binding energy. ZnO film has undergone extensive metal element doping in order to enhance its electrical and optical capabilities. The atomic substitution of Al for Zn results in a free electron in the conduction band, which will increase its transparency and lower its electrical resistivity [20,21]. Aluminum oxide's distinct physical properties have favored its use in a variety of technologies, including photocatalysts, thermal mirrors, and gas sensors [22,23].

Nosocomial infections, which are often commonly referred to as healthcare-related illnesses, represent a significant task in medical facilities, causing increased mortality and morbidity among patients around the world. The root of this problem is microbial colonization and development on the surface of biomedical implants and equipment [24]. Numerous harmful bacterial strains have been commonly found inhabiting medical devices and surfaces, and they are easily spread to patients during routine medical procedures [25,26]. The most frequent bacteria causing nosocomial infection include the gram-negative bacteria *Pseudomonas aeruginosa*, *Escherichia coli*, and *Klebsiella pneumonia*, as well as the gram-positive bacterium *Staphylococcus aureus*. Antimicrobial resistance is an inevitable evolutionary process that has been looming for decades, posing serious difficulties for all global healthcare systems. The World Health Organization (WHO) reported that antimicrobial resistance had caused 700,000 fatalities by 2019, and this number tends to increase to 20 million by 2050 [27]. To overcome such a dilemma, the bactericidal repercussions of Al_2O_3, $CoAl_2O_4$, and $Zn_{0.9}Al_{0.1}O$ nanoparticles in healthcare facilities' ceramics can be used to avoid the spread of nosocomial infections, in public and educational buildings to boost the hygienic situation, and in all kitchens, floors, and bathrooms to encourage hygiene. However, the risk and toxicity of inhaled nanoparticles on humans rely on the duration of exposure and the chemical components, that may be harmful if breathed as nanoparticles. Among these toxicity risks, oxidative stress and inflammation are considered to be at the top of the of the list [28].

In the following investigation, co-precipitation was used to create aluminum oxide (Al_2O_3), cobalt aluminum oxide ($CoAl_2O_4$), and aluminum-doped zinc oxide ($Zn_{0.9}Al_{0.1}O$) nanoparticles. These nanoparticles' antimicrobial potential was then assessed by the disk diffusion method and time-kill assay against a variety of pathogenic bacteria, mostly nosocomial pathogens.

2. Materials and methods

2.1. Synthesis of oxides

Analytical-grade standards of zinc chloride ($ZnCl_2$), aluminum chloride ($AlCl_3$), cobalt chloride ($CoCl_2.6H_2O$), and sodium hydroxide (NaOH) were bought from Fluka, Germany, for the manufacture of Al_2O_3, $CoAl_2O_4$, and $Zn_{0.9}Al_{0.1}O$ nanoparticles using a simple co-precipitation process. For the fabrication of $Zn_{0.9}Al_{0.1}O$ nanostructures, 0.9 M $ZnCl_2$ solution and 0.1 M $AlCl_3$ solution were mixed in distilled water for 15 min. The pH of the aforementioned solution was then adjusted to be lower than 13 using acidic solution drop by drop to obtain the material in the precipitated form. After correcting the pH, the resulting solution was agitated and heated for 2 h. Following that, the precipitate was extensively washed with distilled water to bring its pH value back to neutral. The same procedure as previously described was used to create $CoAl_2O_4$ nanoparticles, but the molar ratios used were 2 M aluminum chloride and 1 M cobalt chloride. The same technique was followed for Al_2O_3 nanostructures, except that 2 M NaOH was added to 1 M aluminum chloride, and after lowering the pH to around 13, the resultant solution was mixed and heated overnight to generate a

creamy solution. All precipitate samples were dried in an oven at 100 °C for 2 h before being pulverized into powder. The samples were calcined for 4 h at 550 °C in a chamber furnace.

2.2. Characterization of nanoparticles

XRD (Bruker D8 Focus X-ray Diffractometer) and Cuk_{α}-radiation ($\lambda = 1.54056$ Å) in the $25^{\circ} \leq 2\theta \leq 75^{\circ}$ range were used to identify the crystalline phases in the samples. The Debye-Scherrer equation was used to calculate the crystallite size of each sample. A TEM was used to investigate particle size and shape (JOEL JEM-100CX). The ultraviolet–visible spectrophotometer V-670, at scan speed 100 nm/min in the range 200–700 nm, was used to analyze the optical absorption of Al_2O_3, $CoAl_2O_4$, and $Zn_{0.9}Al_{0.1}O$ nanoparticle suspension obtained by ultrasonic dispersion of 0.01 g of the sample powder in 10 ml of distilled water for 15 min. The samples' FTIR spectra were acquired using an FTIR 8400S Shimadzu spectrophotometer with KBr pellets in the 400 cm^{-1} and 4000 $cm\text{-}^{1}$ bands.

2.3. Disk diffusion method

Following Clinical and Laboratory Standards Institute (CLSI) recommendations, the Kirby-Bauer disc diffusion technique was performed to assess the sensitivity of the isolates to manufactured nanoparticles. Müller-Hinton agar plates were incubated with freshly produced cultures. Each bacterial suspension's turbidity was calculated by selecting four to five colonies with a sterile loop, mixing with 5 mL of sterile saline, and comparing to a 0.5 McFarland standard. The optical density of the 0.5 McFarland standard is equivalent to the density of a bacterial solution, which is around 1.5×10^8 colony-forming units per milliliter (CFU/mL). The fungal suspensions were spectrophotometrically adjusted to optical densities ranging from 0.09 to 0.11 at 530 nm. The inoculum concentration varied from 0.4×10^6 to 5×10^6 CFU/mL. Using sterile forceps, the sterile paper discs (whatman No. 1, 6 mm in diameter) soaked in 15 μl sterile Al_2O_3, $CoAl_2O_4$, and $Zn_{0.9}Al_{0.1}O$ stock suspensions. were deposited on the surface of the media that had been inoculated with bacterial and fungal suspensions and incubated at 35 ± 2 °C for 16–18 h, with the mean width of inhibitory zones recorded in millimeters. For *Staphylococcus* species, vancomycin was used as a positive control, while ciprofloxacin was used for the remaining bacterial strains. For fungal isolates, clotimazole was utilized as a positive control. The Clinical and Laboratory Standard Institute guidelines were used to interpret the data.

2.4. Determination of minimum inhibitory concentration (MIC) and minimum bactericidal concentration (MBC)

Using batch cultures with varied dosages of the three Nps in suspension, the lowest concentration of nanoparticles that restricts organism growth was reported. After introducing the NPs, 50 mL of Müller-Hinton medium (in 250-mL sterile side-arm Erlenmeyer flasks) were sonicated for 15 min to preclude NPs aggregation. After that, the flasks were inoculated with 1 mL of freshly prepared bacterial suspension to achieve an initial bacterial concentration of 10^8 colony-forming units per milliliter and cultured in an orbital shaker at 200 rpm and 30 °C. Throughout the incubation phase, the high rotational shaking speed was implemented to limit Nps aggregation and boost settling. A lower rpm setting during incubation may result in an underestimation of the antibacterial activity of the NPs. The trials also included a positive control (a flask containing Nps and nutritional medium but no inoculum) and a negative control (a flask containing inoculum and nutritional medium devoid of NPs). The negative controls indicated a microbial growth trend in the absence of NPs. The minimum inhibitory concentration (MIC) was computed as the lowest concentration of Nps that resulted in no turbidity throughout incubation and was expressed in μg/mL. Bacterial cells were cultivated for 24 h in the presence of NPs that suppressed bacterial growth at the least bactericidal concentration, followed by dispersion and reculturing on Müller-Hinton plates to figure out the minimal bactericidal concentration. The plates were then kept at 37 °C overnight [29].

2.5. Time kill study

The death rate of bacterial strains by a prescribed antibacterial agent was assessed at various time periods. The time-kill curve test was performed in accordance with the method described in CLSI's M26-A document (Barry et al., 1999). The experiment was carried out in flasks containing 20 mL of MHB inoculated with 5×10^5 CFU/mL and supplemented with the necessary amounts of Al_2O_3, $CoAl_2O_4$, and $Zn_{0.9}Al_{0.1}O$ (MICx1, MICx2, and MICx4). The flasks were shaken at 150 rpm in 37 °C conditions. The OD_{600nm} of the cultures was monitored every 2 h after inoculation, with the final value reported after 24 h. To minimize unnecessary optical noise generated by the light scattering features of the NPs all through optical measurements of the growing cultures, the very same liquid medium lacking bacterial inoculum but possessing the same concentration of NPs cultured under identical conditions served as a blank control.

2.6. Transmission electron microscope

The impact of aluminum-doped zinc oxide nanoparticles was verified using a transmission electron microscope depending on MIC values and time-kill curve data (JEM-1400 Plus). A universal electron microscope fixative was used to fix cells of untreated (control) and treated *E. coli*. Ethyl alcohol and propylene oxide were applied for dehydration. The pellets were implanted in capsules and polymerized before thin slices were produced using a LKB 2209-180 ultra-microtome and stained for 30 min with uranyl acetate and 2 min with lead acetate. A similar strategy was used to control bacterial cells. Cells were examined at magnifications of 20000× and 25000 x with an accelerating voltage of 80 KV.

2.7. Statistical analysis

The means ± standard errors (S.E.M.) were used to present all the data. The F-statistic of a one-way analysis of variance (ANOVA) was used to evaluate the significance of differences between research. The Scheffé, Bonferroni, Holm, and Tukey HSD tests are the subsequent multiple comparison tests. Which of the treatment pairs differ significantly from one another would probably be determined by these post-hoc tests. The two-tailed p-value was used to determine the statistical significance threshold. It was considered significant at a level of <0.05 and highly significant at a level of <0.001. All experiments were accomplished using three trials to ensure accuracy.

3. Result and discussion

3.1. Characterization of oxides

Fig. 1 depicts the XRD patterns of Al_2O_3, $CoAl_2O_4$, and $Zn_{0.9}Al_{0.1}O$ nanoparticles generated by the co-precipitation technique. Fig. 1 (a) depicts an XRD pattern of fabricated alumina nanoparticles featuring three primary peaks positioned at 2θ values of 37.71°, 45.86°, and 66.97°, correlating to the planes (311), (400), and (440), respectively. Fig. 1 (b) depicts the XRD pattern of $CoAl_2O_4$ nanoparticles exhibiting 5 major diffraction peaks with 2θ values of 31.3°, 36.89°, 44.69°, 59.19°, and 65.4°, relating to the (220), (311), (400), (511), and (440) planes, respectively. In Fig. 1 (c), $Zn_{0.9}Al_{0.1}O$ nanoparticles exhibit 9 major diffraction peaks at 2θ values of 31.8°, 34.45°, 36.28°, 45.57°, 56.63°, 62.88°, 66.42°, 67.98°, and 69.11°, corresponding to the (100), (002), (101), (102), (110), (103), (200), (112), and (201) planes, respectively. According to the Joint Committee on Powder Diffraction Standards (JCPDS) card nos. 29–63, 44–0160, and 36–1451, these planes are associated with γ -alumina, spinel types $CoAl_2O_4$ with cubic structures, and Al–ZnO with conventional hexagonal wurtzite structure [30–34]. The sharpness and intensity of the peaks of Al_2O_3, $CoAl_2O_4$, and $Zn_{0.9}Al_{0.1}O$ show that the produced NPs are well-crystalline. Furthermore, no typical impurity phase peaks are detected.

The average lattice parameter (a) of Al_2O_3 and $CoAl_2O_4$ NPs synthesized via co-precipitation is derived using Bragg's law as stated below and depicted in Table 1.

$$a = d\sqrt{h^2 + k^2 + l^2} \tag{1}$$

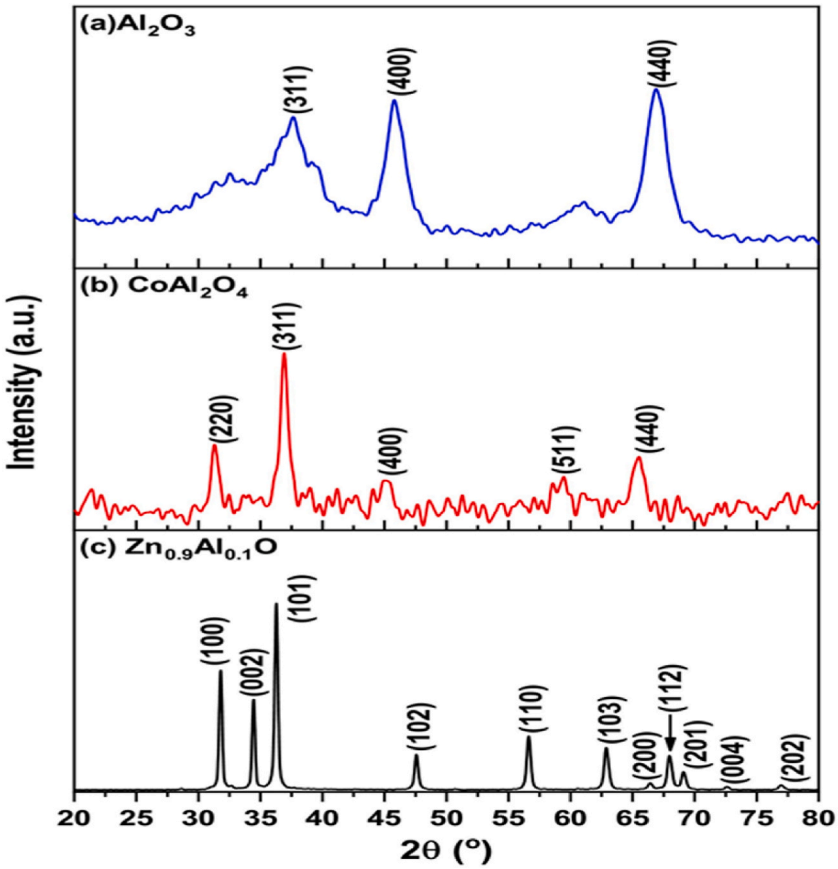

Fig. 1. XRD patterns of co-precipitated (a) Al_2O_3, (b) $CoAl_2O_4$, and (c) $Zn_{0.9}Al_{0.1}O$ NPs.

Due to the pure hexagonal wurtzite structure of the $Zn_{0.9}Al_{0.1}O$ NPs, the lattice parameters a and c are calculated using the following formula:

$$\frac{1}{d^2}=\frac{4}{3}\left(\frac{h^2+hk+k^2}{a^2}\right)+\frac{l^2}{c^2} \quad (2)$$

Where a and c are the lattice parameters in Å, d is the inter-planer distance in Å, and (h, k, and l) are the Miller indices.

The average size of the crystallites of Al_2O_3, $CoAl_2O_4$, and $Zn_{0.9}Al_{0.1}O$ NPs generated by the co-precipitation approach was derived using the Debye-Scherrer equation below [35,36] based on the entire width at half maximum of the recorded diffraction peaks and shown in Table 1.

$$D=\frac{K\lambda}{\beta_{hkl}\cos\theta^{\circ}} \quad (3)$$

D is the average crystallite size in nm, *K* is a constant or shape factor and equals to 0.9, λ is the wavelength of the X-ray radiation, βhkl is the peak width at half maximum intensity and θ is the peak position.

The TEM images and particle size histograms of co-precipitated Al_2O_3, $CoAl_2O_4$, and $Zn_{0.9}Al_{0.1}O$ NPs were depicted in Fig. 2. The TEM pictures (Fig. 2(a–c)) reveal that the processed composites are composed of distinct, homogeneous, and almost spherical nanoparticles. The resultant particle size histograms (Fig. 2(d–f)) matched the lognormal distribution profile, and the average particle size values obtained are presented in Table 1. The particle sizes determined by TEM correspond well with the crystalline sizes determined by the XRD method.

In the process of investigating how wavelength affected the charting of the absorbance spectra of the co-precipitated Al_2O_3, $CoAl_2O_4$, and $Zn_{0.9}Al_{0.1}O$ NPs, Fig. 3 demonstrates the findings obtained. Fig. 3 (a) and (c) depict the ultraviolet–visible absorption spectra of the materials Al_2O_3 and $Zn_{0.9}Al_{0.1}O$, respectively. Al_2O_3 material exhibit a large absorption peak at wavelength of 239 nm which is in accordance with Piriyawong et al. [10]. Similarly, $Zn_{0.9}Al_{0.1}O$ showed a large absorption peak at wavelength of 372 nm, illustrating the findings of Alkahlout et al. [37] and Ahammed et al. [38]. These spectra revealed no further peaks, revealing the purity of the Al_2O_3 and $Zn_{0.9}Al_{0.1}O$ NPs' production. The $CoAl_2O_4$ NPs, on the other hand, exhibit two absorption peaks at wavelengths of 261 nm and 473 nm in their ultraviolet–visible absorption spectra, which is depicted in Fig. 3(b). Analysis using ultraviolet (UV) spectroscopy revealed a symmetrical shift of the absorption edge towards the shorter wavelength.

FTIR spectra of Al_2O_3, $CoAl_2O_4$, and $Zn_{0.9}Al_{0.1}O$ NPs prepared by the co-precipitation method are illustrated in Fig. 4 in the range of 4000–400 cm^{-1}. Fig. 4 (a) depicts the FTIR spectrum of Al_2O_3 NPs, which is categorized by a broad, unresolved band between 500 and 800 cm^{-1}, with two peak values at 589.15 cm^{-1} and 778.62 cm^{-1} that may be traced back to the stretching vibrations of AlO_6 and AlO_4, which is in accordance with Manyasree et al. [35]; Fig. 4 (b) portrays two sharp bands at 666.77 cm^{-1} and 563.1 cm^{-1}, which coincide to the spinel-like structure of $CoAl_2O_4$ with Al^{3+}cations, as stated by Khassin et al. [39]. Referring to previous studies performed by Torkian & Daghighi [40] and Gholami et al. [41], the peak obtained in our study at 666.77 cm^{-1} is linked to AlO_6 vibrations, whereas the peak at 563.1 cm^{-1} is related to CoO_4 vibrations. The peaks at ~449.81 cm^{-1} and ~668.7 cm^{-1} in the FTIR spectrum of $Zn_{0.9}Al_{0.1}O$ NPs, depicted in Fig. 4(c), are indicative of the symmetric and asymmetric Zn–O vibrations, respectively [38]. For Al_2O_3, $CoAl_2O_4$, and $Zn_{0.9}Al_{0.1}O$ NPs, the FTIR spectra indicate a band from 1500 cm^{-1}–1750 cm^{-1}, centered at 1636.79 cm^{-1}, 1637.27 cm^{-1}, and 1649.80 cm^{-1}, respectively. This peak is attributed to the bending vibrations of H–*O*–H, which are driven by the presence of physisorbed water.

3.2. Disk diffusion method

The disk diffusion method was employed to investigate the susceptibility of several bacterial pathogens to nanosuspensions, and the findings are shown in Fig. 5. To successfully report NPs antibacterial activity, a distinct inhibition zone should be created around the nanosuspensions. In terms of the type of nanoparticles produced by the co-precipitation approach, aluminum-doped zinc oxide nanoparticles had the highest antibacterial activity in comparison to all other nanoparticle treatments ($p < 0.01$). There was no significant difference in the antibacterial properties of the other nanoparticles produced (aluminum oxide and cobalt aluminum oxide). The inhibition zones for $Zn_{0.9}Al_{0.1}O$ were 14 mm, 13 mm, 12 mm, and 14 mm against *E. coli*, *K. pneumoniae*, *P. aeruginosa*, and *S. aureus*, respectively. $CoAl_2O_4$ NPs had reduced antibacterial activity, with inhibition zones of 9 mm, 9 mm, 10 mm, and 11 mm against *E. coli*, *K. pneumoniae*, *P. aeruginosa,* and *S. aureus*, respectively. The antibacterial activity of Al_2O_3 NPs reflected an inhibition zone of 12 mm, 11 mm, 9 mm, and 11 mm for *E. coli*, *K. pneumoniae*, *P. aeruginosa,* and *S. aureus*, respectively. Referring to our findings, it was clear that

Table 1
The average size and lattice parameter of Al_2O_3, $CoAl_2O_4$, and $Zn_{0.9}Al_{0.1}O$ NPs synthesized via co-precipitation.

Characterization Method			Sample		
			Al_2O_3	$CoAl_2O_4$	$Zn_{0.9}Al_{0.1}O$
XRD	Lattice parameter a	(Å)	7.91	8.05	3.2
	Lattice parameter c	(Å)	–	–	5.4
	Average crystallite size	(nm)	4.6	11.5	24.3
TEM	Average particle size	(nm)	4.1	9.5	31.6

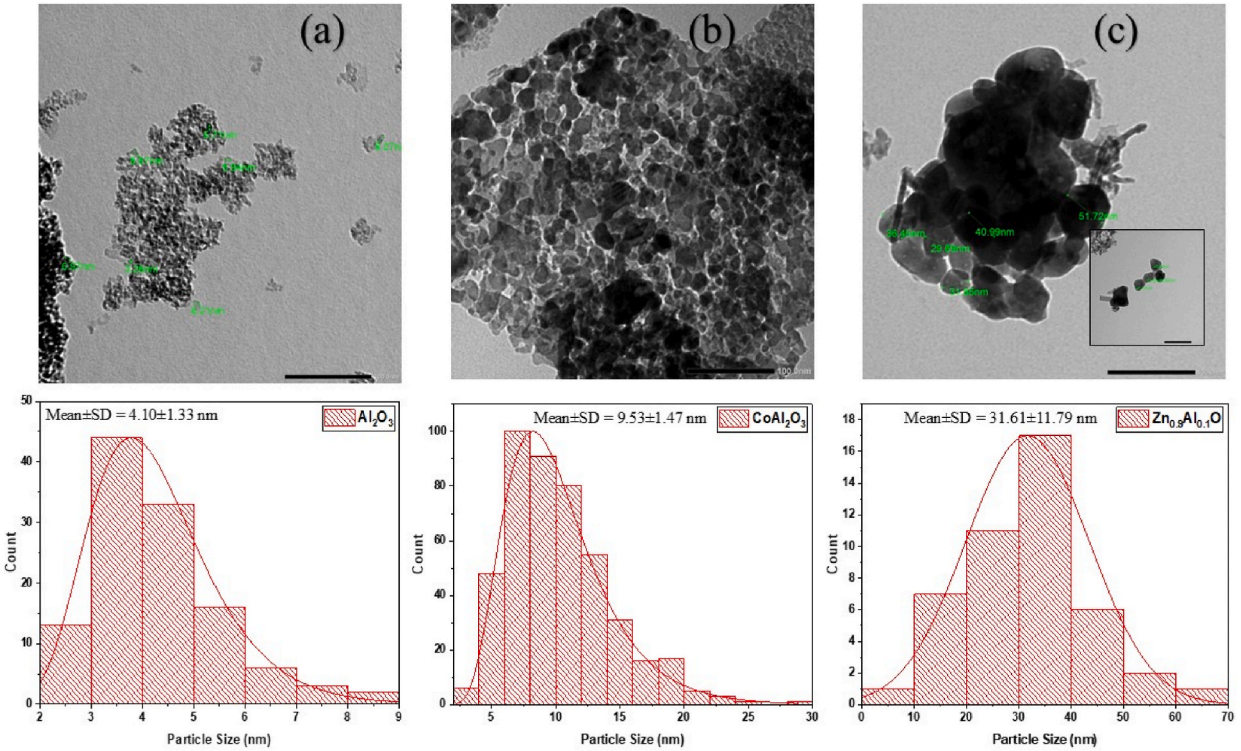

Fig. 2. TEM images of (a) Al_2O_3, (b) $CoAl_2O_4$ and (c) $Zn_{0.9}Al_{0.1}O$ NPs with the particle size histograms depicted in (d–f).

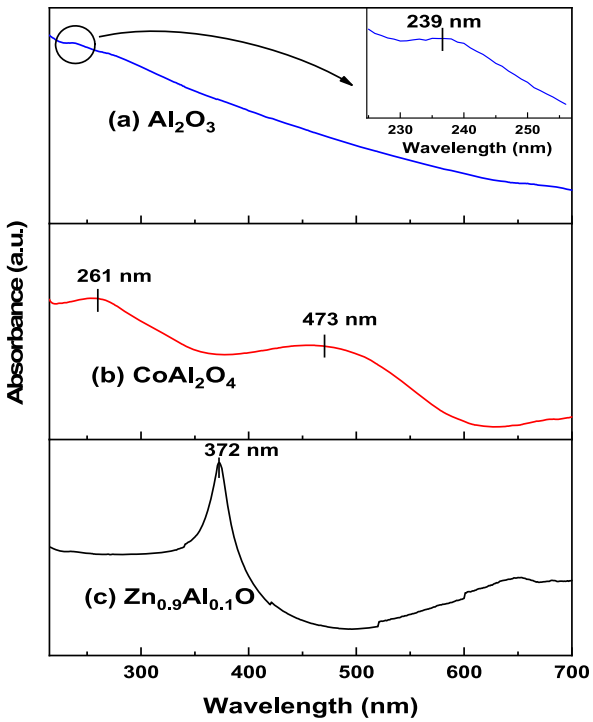

Fig. 3. UV–visible absorption spectra for (a) Al_2O_3, (b) $CoAl_2O_4$, and (c) $Zn_{0.9}Al_{0.1}O$ NPs prepared by the co-precipitation method.

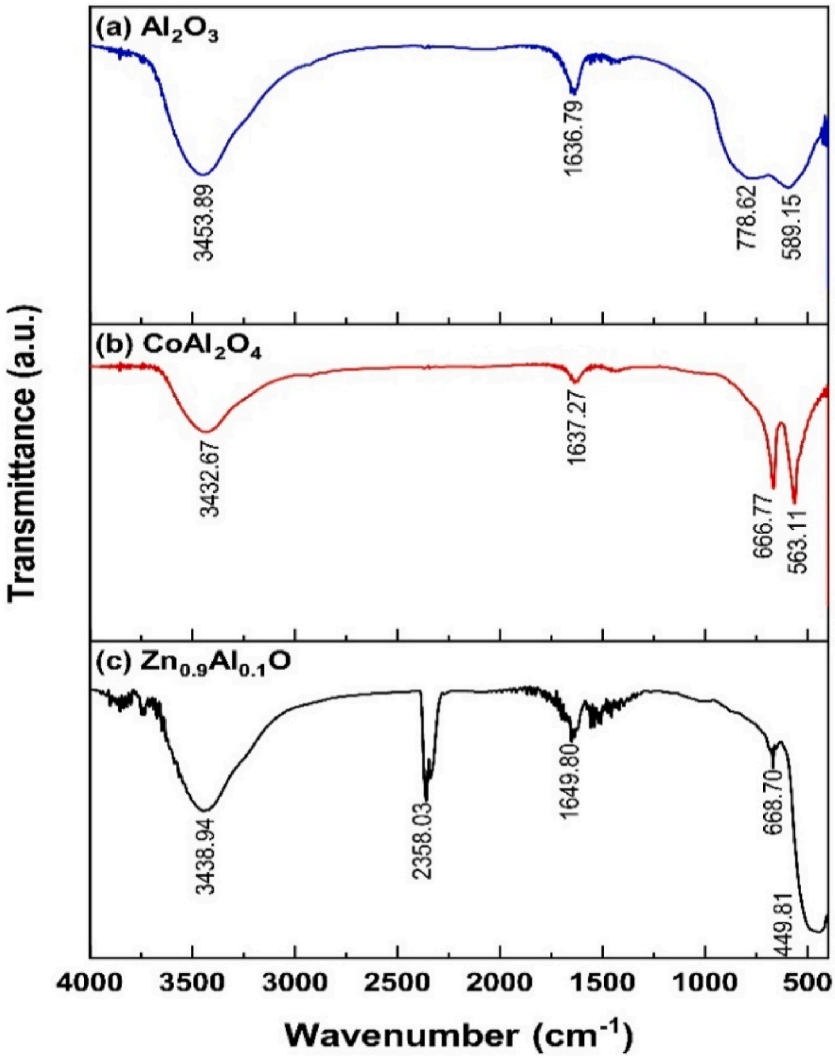

Fig. 4. FTIR spectra for (a) Al_2O_3, (b) $CoAl_2O_4$, and (c) $Zn_{0.9}Al_{0.1}O$ NPs prepared by co-precipitation.

$Zn_{0.9}Al_{0.1}O$ and Al_2O_3 had the highest antimicrobial activity against the gram-negative *E. coli* bacteria, and that activity decreased when dealing with *K. pneumoniae* and *P. aeruginosa* ($p < 0.01$). The inhibition zone diameters detected against *S. aureus* were 11 mm, 11 mm and 14 mm for Al_2O_3, $CoAl_2O_4$ and $Zn_{0.9}Al_{0.1}O$, respectively. These results show no distinction between gram-positive and gram-negative bacteria ($p < 0.01$). Several studies have been conducted to assess the antibacterial activity of Al_2O_3 and ZnO nanoparticles against both gram-negative and gram-positive bacteria strains, all of which rely on the fact that metal oxide nanoparticles may limit the growth of *E. coli* and *S. aureus* [35,42,43]. According to Manyasree et al. [35], the largest zone of inhibition by Al_2O_3 was 9 mm for *E. coli* and a lesser zone of inhibition of 6 mm for *S. aureus*. However, Ahmad et al. [43] found that the zone of inhibition induced by ZnO nanoparticles varied from 16 to 18 mm for gram-negative bacteria (*Escherichia coli, Klebsiella pneumonia, and Pseudomonas aeruginosa*) and from 18 to 21 mm for gram-positive bacteria.

3.3. Determination of minimum inhibitory concentration (MIC) and minimum bactericidal concentration (MBC)

In the course of studying the antimicrobial activity of Al_2O_3, $CoAl_2O_4$, and $Zn_{0.9}Al_{0.1}O$ NPs against *Escherichia coli*, *Klebsiella pneumoniae*, *Pseudomonas aeruginosa,* and *Staphylococcus aureus,* the minimum inhibitory concentrations (MIC) and minimum bactericidal concentrations (MBC) were conducted, and the results were reported in Table 2. Results showed that the MIC values of the produced nanoparticles varied from 4000 μg/mL to 16000 μg/mL. Al2O3 nanoparticles had MIC values of 12000 μg/mL, 15000 μg/mL, 16000 μg/mL, and 14000 μg/mL against *E. coli*, *K. pneumoniae*, *P. aeruginosa,* and *S. aureus*, respectively. Furthermore, CoAl2O4 nanoparticles had MIC values of 8000 μg/mL, 10000 μg/mL, 10000 μg/mL, and 8000 μg/mL against *E. coli*, *K. pneumoniae*, *P. aeruginosa*, and *S. aureus*, respectively. Besides that, the MIC values of $Zn_{0.9}Al_{0.1}O$ nanoparticles achieved against *E. coli*, *K. pneumoniae*, *P. aeruginosa,* and *S. aureus* were 4000 μg/mL, 6000 μg/mL, 6000 μg/mL, and 4000 μg/mL, respectively. Concerning the

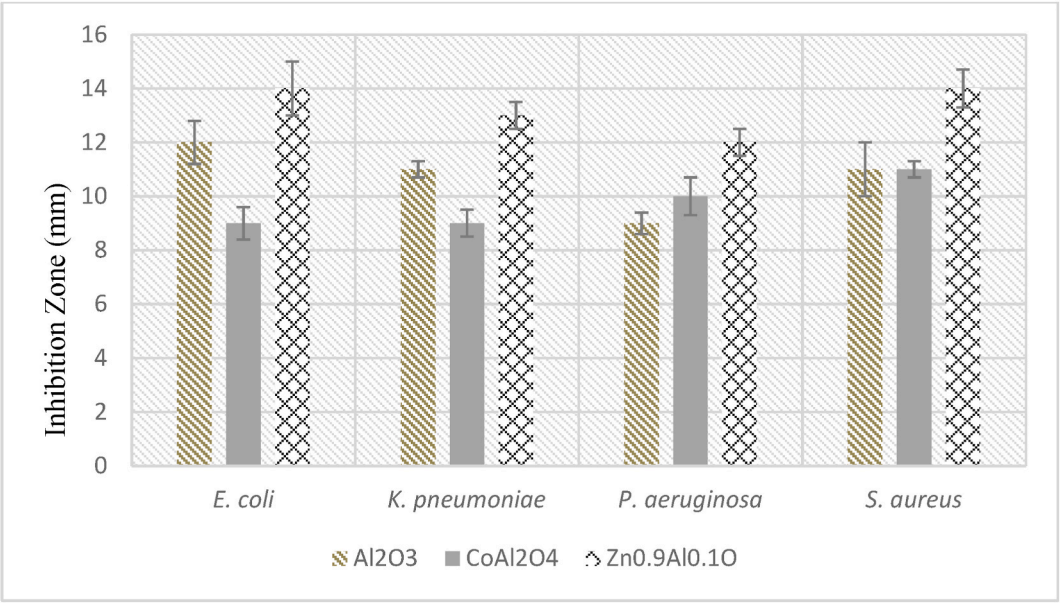

Fig. 5. Histogram showing the mean diameters of inhibition zones recorded for Al_2O_3, $CoAl_2O_4$, and $Zn_{0.9}Al_{0.1}O$ NPs prepared by the co-precipitation method.

Table 2
Minimum inhibitory concentration (MIC) and minimum bactericidal concentration recorded for co-precipitated Al_2O_3, $CoAl_2O_4$, and $Zn_{0.9}Al_{0.1}O$ NPs against different bacterial strains.

pathogens	MIC (μg/mL)			MBC (μg/mL)			MIC index MBC/MIC		
	Al_2O_3	$CoAl_2O_4$	$Zn_{0.9}Al_{0.1}O$	Al_2O_3	$CoAl_2O_4$	$Zn_{0.9}Al_{0.1}O$	Al_2O_3	$CoAl_2O_4$	$Zn_{0.9}Al_{0.1}O$
E. coli	12000	8000	4000	–	24000	8000	–	3	2
K. pneumoniae	15000	10000	6000	–	40000	12000	–	4	2
P. aeruginosa	16000	10000	6000	–	40000	12000	–	4	2
S. aureus	14000	8000	4000	–	24000	8000	–	3	2

MBC of the synthesized NPs, Al_2O_3 NPs did not show any exceptional results when tested against the four bacterial strains. For that of $CoAl_2O_4$ NPs, the MBC values documented against *E. coli* and *S. aureus* were equivalent to that of MICx3; MBC were equivalent to MICx4 in the case of *K. pneumoniae* and *P. aeruginosa.* When testing the MBC for $Zn_{0.9}Al_{0.1}O$ NPs, it was clear that the values were twice that of the MIC when tested against *E. coli*, *K. pneumoniae*, *P. aeruginosa,* and *S. aureus.* Based on the MIC index derived in Table 2, $CoAl_2O_4$ and $Zn_{0.9}Al_{0.1}O$ NPs have been shown to exhibit a bactericidal effect on the tested microorganisms ($p < 0.01$). In this context, earlier investigations revealed varying MIC and MBC values for metal oxide NPs [35,36]. Manyasree et al. [31] revealed that the MIC of Al_2O_3 for *E. coli* and *S. aureus* was 4 mg/mL. In contrast to our findings, Klink et al. [36] observed a low MIC for *S. aureus* (6.25 mg/mL) and a high MIC for *E. coli* (25 mg/mL). In addition, Pasquet et al. [44] reported that the MBC values of ZnO NPs recorded 18 μg/mL, 14 μg/mL, and 16 μg/mL for *E. coli, P. aeruginosa,* and *S. aureus,* respectively. Because resistance to conventional antimicrobial agents has been growing, even towards those recognized as the superweapon against certain infections as reported by multiple studies, the use of these NPs can outperform their use, even at the high concentrations required to inhibit and kill the bacterial strains [45,46].

3.4. Time-kill study

The time-kill study has been commonly employed to assess the concentration level of an antimicrobial agent with bactericidal properties. Such bactericidal activity can be exploited in the treatment of bacterial infections in concentration and time-dependent manner [47]. It is an effective technique to study the dynamic interaction between the antimicrobial agent under study and the microbial strain [48]. MHB were used to test the antimicrobial activity of three concentrations of each nanoparticle Al_2O_3, $CoAl_2O_4$, and $Zn_{0.9}Al_{0.1}O$ (MIC X 1, MIC X 2 and MIC X 4). Each bacterium's growth pattern in culture conditions lacking nanoparticles was employed as a control. Figs. 6–8 demonstrate the antibacterial activities of the tested concentrations (MIC X 1, MIC X 2, and MIC X 4) of Al_2O_3, $CoAl_2O_4$, and $Zn_{0.9}Al_{0.1}O$ NPs, respectively, against *Escherichia coli* (A1), *Klebsiella pneumoniae* (B1), *Staphylococcus aureus* (C1), and *Pseudomonas aeruginosa* (D1) after being cultivated in MHB and incubated at 37 °C for 24 h.

After monitoring the growth of Al_2O_3-treated bacterial isolates in culture media for 24 h, it was clear that the growth was reduced significantly ($p < 0.01$) in comparison to the positive control. On the other hand, monitoring bacterial growth in culture media

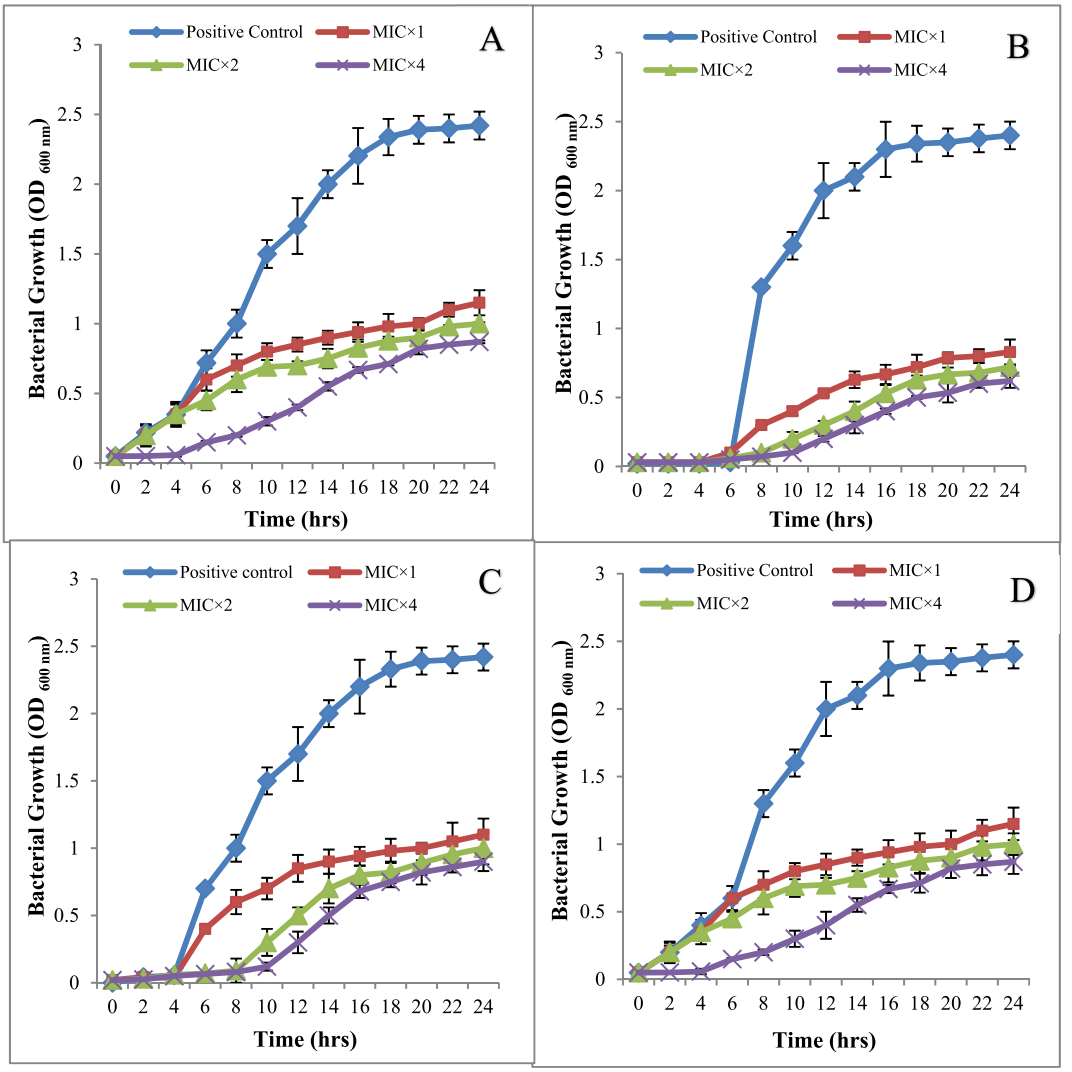

Fig. 6. Effect of MIC × 1, MIC × 2 and MIC × 4 of Al_2O_3 NPs on *Escherichia coli* (A), *Klebsiella pneumoniae* (B), and *Staphylococcus aureus* (C), and *Pseudomonas aeruginosa* (D) cultivated in MHB during different time intervals.

(supplemented with varying amounts of $CoAl_2O_4$ and $Zn_{0.9}Al_{0.1}O$ NPs) revealed that bacterial growth was nearly totally suppressed ($p < 0.01$). All amounts tested were efficient at inhibiting bacterial growth ($p < 0.01$). MIC X 4 was the most powerful antibacterial therapy among the three concentrations of the tested nanoparticles generated ($p < 0.01$), followed by MIC X 2 and MIC X 1. As a result of these findings, the antibacterial activity of Al_2O_3, $CoAl_2O_4$, and $Zn_{0.9}Al_{0.1}O$ NPs was concentration-dependent. Our findings are consistent with those of Sirelkhatim et al. [49] and Ahmad et al. [39], who found that ZnO NPs displayed concentration-dependent bactericidal action against *Escherichia coli*, *Klebsiella pneumoniae*, *Pseudomonas aeruginosa*, and *Staphylococcus aureus*. Moreover, many studies have found that Al_2O_3 at different concentrations can cause a growth delay in all tested strains of S. aureus [43,49].

3.5. Transmission electron microscope

The morphological alterations in *Escherichia coli* cells after exposure to $Zn_{0.9}Al_{0.1}O$ NPs were seen using TEM microscopy. Based on the micrographs obtained from the TEM, which are shown in Fig. 9 at 20000x A1 and 25000x A2 magnification, it is clear that the shape of the untreated cell, its wall, and intracellular structures were intact. In contrast, $Zn_{0.9}Al_{0.1}O$ NPs-treated *Escherichia coli* cells were deformed. At magnifications of 20000× B1 and 250000x B2, the TEM pictures clearly showed the change in cell shape, in addition to the alteration and disintegration of bacterial cell wall morphology, the cytoplasmic membrane, and protoplasm. In addition, it is obvious that the cell witnessed a leakage in the protoplasm. According to these observations, $Zn_{0.9}Al_{0.1}O$ Nps deformed and destroyed the bacterial cell wall and cytoplasmic membrane, resulting in protoplasm leakage and cell death. These results are in accordance with those of Liang et al. [50], who recorded that the microscopic analysis of bacterial cell surfaces showed alteration after

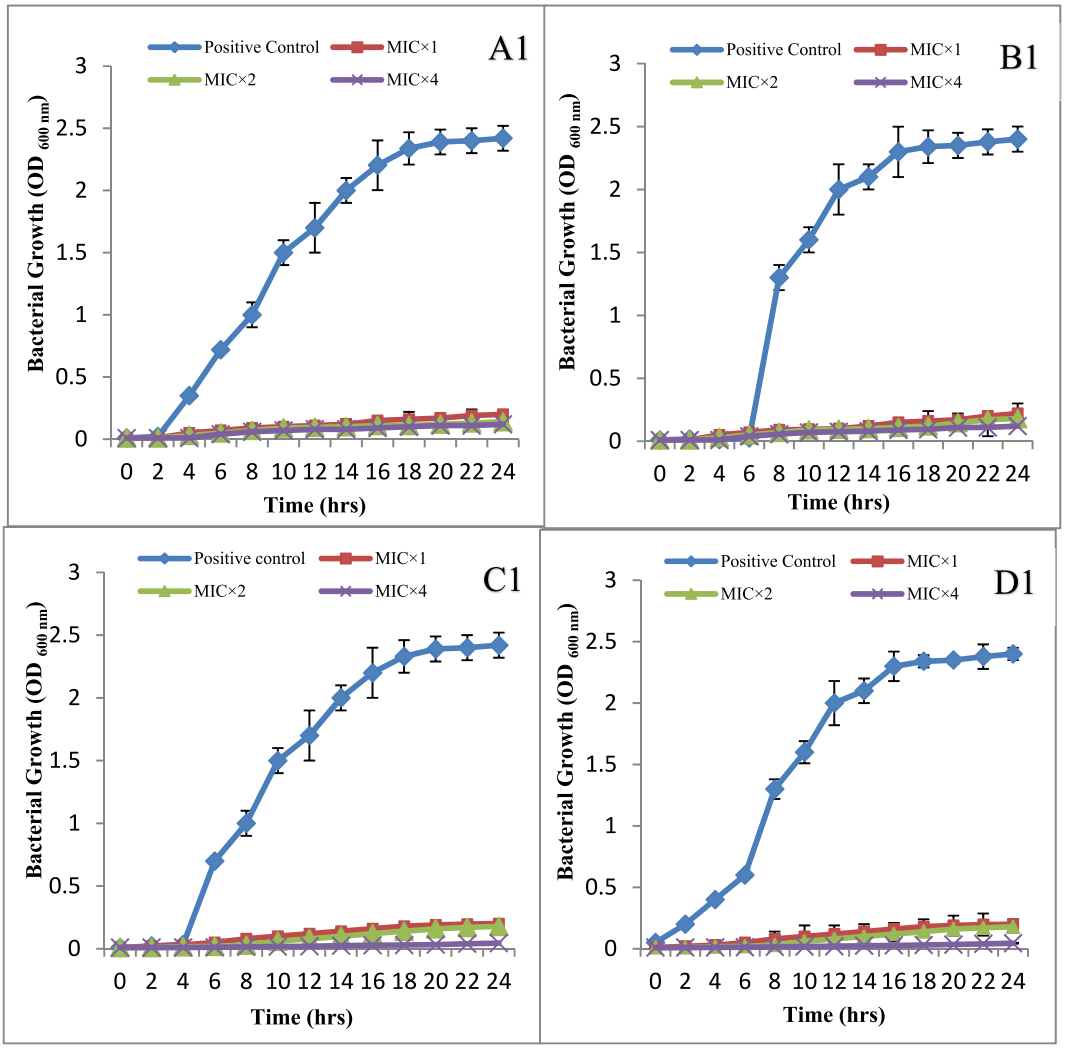

Fig. 7. Effect of MIC × 1, MIC × 2 and MIC × 4 of $CoAl_2O_4$ NPs on *Escherichia coli* (A1*)*, *Klebsiella pneumoniae* (B1), *Staphylococcus aureus* (C1), and *Pseudomonas aeruginosa* (D1) cultivated in MHB during different time intervals.

being treated with ZnO nanoparticles. These nanoparticles adhered to the surface of the bacterial cell and attached to the bacterial cell wall, resulting in the rupture of the membrane. The primary mechanism behind the antimicrobial potential of nanoparticles is not limited to their ability to disrupt microbial membranes. Rather, the ability of nanoparticles to impede biofilm formation, due to its higher surface area-to-mass ratio, is thought to be crucial in the development of bacterial resistance, as it offers refuge and protection to microorganisms, enabling them to escape from most antibiotics and undergo mutations that they can then exchange with other bacterial cells [51].

4. Conclusion

The use of nanomaterials in medicine has grown dramatically over the last decade. Metal nanoparticles have recently been tested for their antimicrobial properties, despite being severely hampered in most industries. The novel aspect of this work lies in the fact that distinct microbial species, including both gram-positive and gram-negative bacteria, was included in the evaluation of the antimicrobial activity of three different nanoparticles in the same study through the use of different antimicrobial testing techniques. It clearly demonstrates the effectiveness of cobalt aluminum oxide ($CoAl_2O_4$) and aluminum-doped zinc oxide ($Zn_{0.9}Al_{0.1}O$) nanoparticles as antimicrobial agents against different pathogens, mainly nosocomial ones. However, Aluminum oxide (Al_2O_3) did not show promising results on its own. These antimicrobial nanoparticles can be incorporated into paints and coated ceramics in food industries and medical facilities, creating a permanent hygiene environment and conquering plenty of infections. In the field of antimicrobial resistance, nanomaterials could be considered the salvation for plenty of infections. However, none of these nanotechnologies can stand alone in facing pathogenic resistance evolution and thus warding off resistant bacterial infections. Since

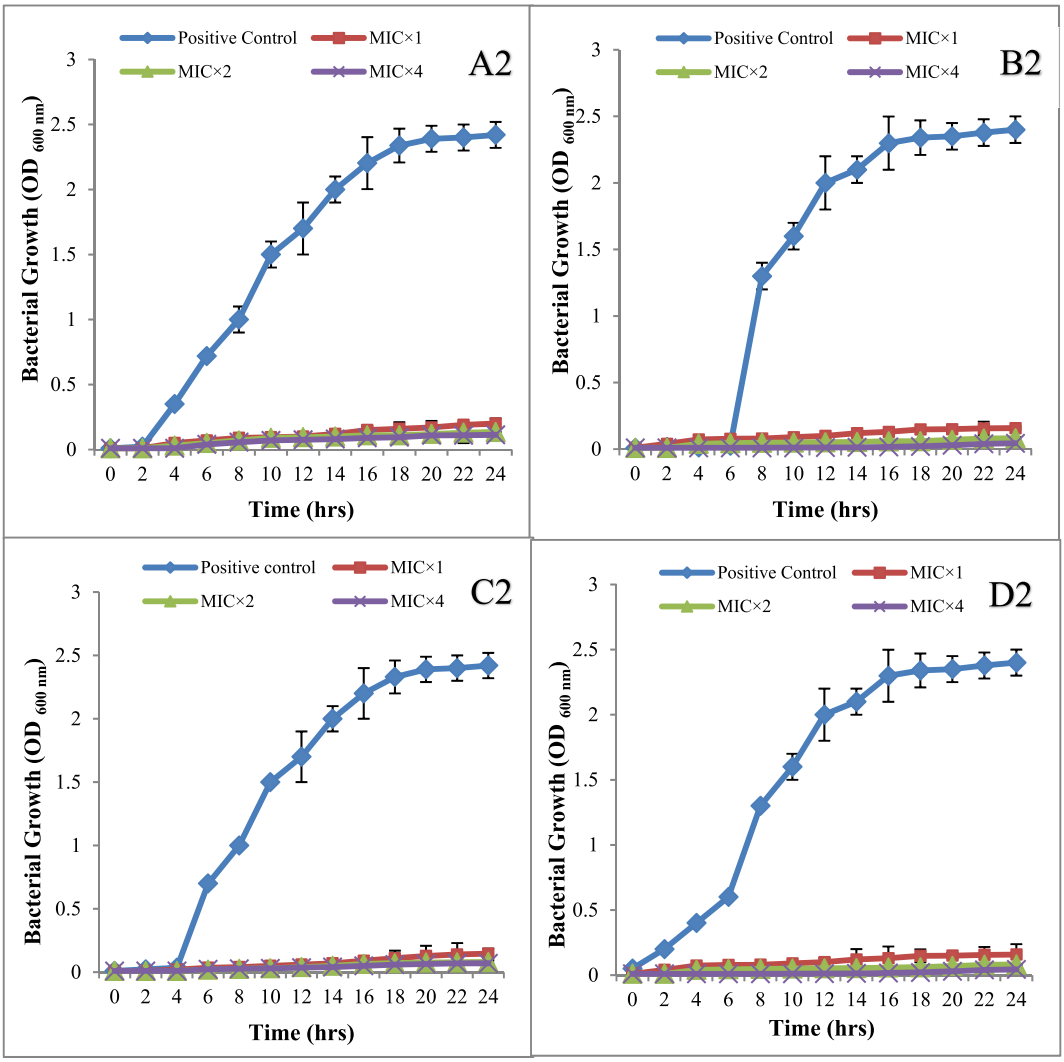

Fig. 8. Effect of MIC × 1, MIC × 2 and MIC × 4 of $Zn_{0.9}Al_{0.1}O$ NPs on *Escherichia coli* (A2), *Klebsiella pneumoniae* (B2), *Staphylococcus aureus* (C2), and *Pseudomonas aeruginosa* (D2) cultivated in MHB during different time intervals.

nanoparticles are smaller (<100 nm), have a consistent size and structure, and are chemically stable, their application as antimicrobials outweighs that of antibiotics. Additionally, by engaging with the efflux pumps that cause resistance to many antimicrobials, nanoparticles can enter the cell membrane of bacteria more effectively than conventional antimicrobial drugs. This may illustrate how antimicrobial medicines can be used in conjunction with nanoparticles to increase their activity and lessen their toxicity to human cells. It is very important to integrate different antimicrobial therapies and end up with a multi-dimensional killing approach mainly through the use of such nanoparticles as carriers for high potential antimicrobial agents to end up with promising bacterial-killing machine. While the previously suggested method shows promise, it presents certain difficulties with regard to the expenses, release, and management of these nanoparticles.

Funding

There has been no significant financial support for this work that could have influenced its outcome.

Ethics approval and consent to participate

Not applicable.

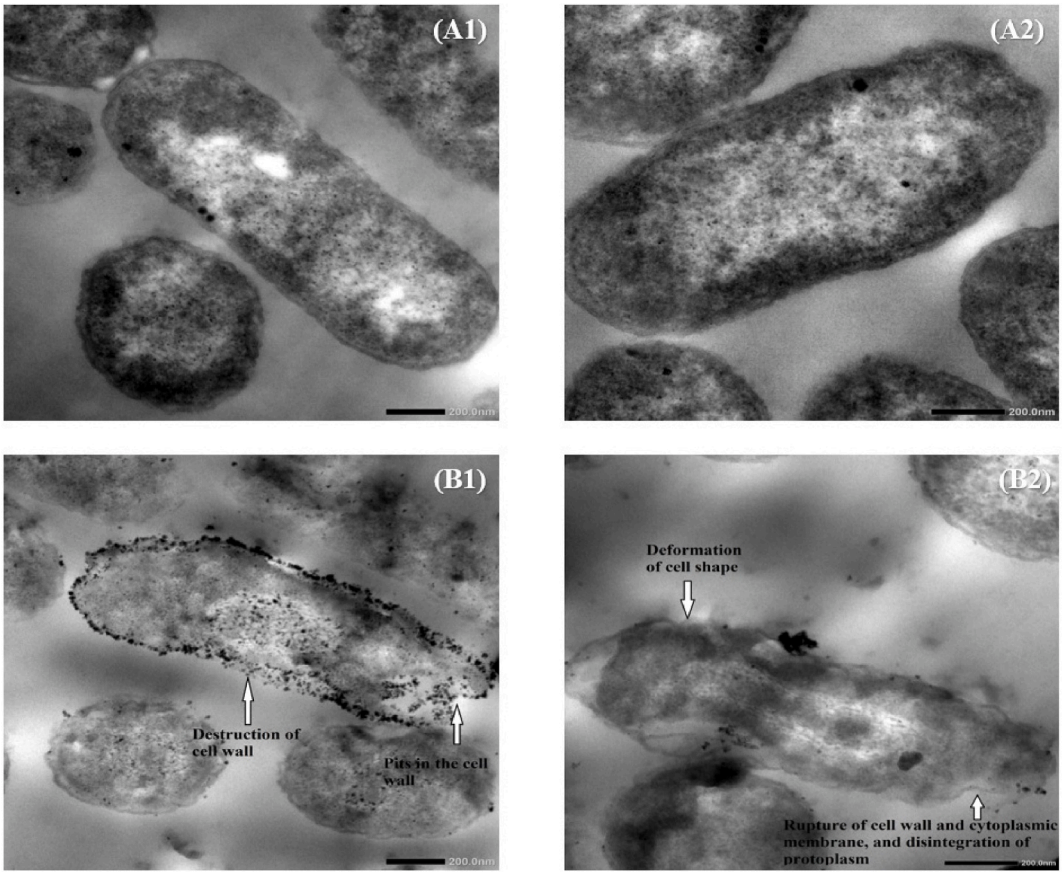

Fig. 9. TEM images for *E. coli*, untreated (A1 & A2) and treated with $Zn_{0.9}Al_{0.1}O$ nanosuspensions (B1 & B2) examined at magnifications 20000× (A1 & B1) and 25000x (A2 & B2).

Consent for publication

All the authors in the article have approval for publication.

Data availability

Data available upon request.

CRediT authorship contribution statement

Mohamad Omeiri: Writing – review & editing, Writing – original draft, Formal analysis, Data curation. **Esraa El Hadidi:** Visualization, Methodology, Investigation, Funding acquisition. **Ramadan Awad:** Project administration, Methodology, Formal analysis, Data curation. **Jamalat Al Boukhari:** Methodology. **Hoda Yusef:** Validation, Supervision, Project administration, Methodology, Formal analysis, Data curation.

Declaration of competing interest

The authors declare that they have no known competing financial interests or personal relationships that could have appeared to influence the work reported in this paper.

Acknowledgments

The authors thank Beirut Arab University (BAU) for their technical support throughout the project.

References

[1] S.P. Deshmukh, S.M. Patil, S.B. Mullani, S.D. Delekar, Silver nanoparticles as an effective disinfectant: a review, Mater. Sci. Eng. C. 97 (2019) 954–965, https://doi.org/10.1016/j.msec.2018.12.102.

[2] N. Spernovasilis, S. Tsiodras, G. Poulakou, Emerging and Re-emerging infectious diseases: humankind's companions and competitors, Microorganisms 10 (2022) 98, https://doi.org/10.3390/microorganisms10010098.

[3] A. Alajlan, L. Mukhtar, A. Almussallam, A. Alnuqaydan, N. Albakiri, T. Almutari, K. Shehail, F. Aldawsari, S. Alajel, Assessment of disinfectant efficacy in reducing microbial growth, PLoS One 17 (6) (2022) e0269850, https://doi.org/10.1371/journal.pone.0269850.

[4] L. Motelica, B.S. Vasile, A. Ficai, A.V. Surdu, D. Ficai, O.C. Oprea, E. Andronescu, D.C. Jinga, A.M. Holban, Influence of the alcohols on the ZnO synthesis and its properties: the photocatalytic and antimicrobial activities, Pharmaceutics 14 (12) (2022) 2842, https://doi.org/10.3390/pharmaceutics14122842.

[5] L. Motelica, O.C. Oprea, B.S. Vasile, A. Ficai, D. Ficai, E. Andronescu, A.M. Holban, Antibacterial activity of solvothermal obtained ZnO nanoparticles with different morphology and photocatalytic activity against a dye mixture: methylene blue, rhodamine B and methyl orange, Int. J. Mol. Sci. 24 (6) (2023) 5677, https://doi.org/10.3390/ijms24065677.

[6] J. Prakash, J. Cho, Y.K. Mishra, Photocatalytic TiO2 nanomaterials as potential antimicrobial and antiviral agents: scope against blocking the SARS-COV-2 spread. Micro, Nanno. Eng. 14 (2022) 100100, https://doi.org/10.1016/j.mne.2021.100100.

[7] N. Kashef, M.R. Hamblin, Can microbial cells develop resistance to oxidative stress in antimicrobial photodynamic inactivation? Drug Resist. Updat. 31 (2017) 31–42, https://doi.org/10.1016/j.drup.2017.07.003.

[8] H. Veisi, S. Azizi, P. Mohammadi, Green synthesis of the silver nanoparticles mediated by thymbra spicata extract and its application as a heterogeneous and recyclable nanocatalyst for catalytic reduction of a variety of dyes in water, J. Clean. Prod. 170 (2018) 1536–1543, https://doi.org/10.1016/j.jclepro.2017.09.265.

[9] R. Kumar, G.R. Pulikanti, K.R. Shankar, D. Rambabu, V. Mangili, L.R. Kumbam, P.S. Sagara, N. Nakka, M. Yogesh, Surface coating and functionalization of metal and metal oxide nanoparticles for biomedical applications, Metal Oxides for Biomedical and Biosensor Applications (2021) 205–231, https://doi.org/10.1016/B978-0-12-823033-6.00007-7.

[10] V. Piriyawong, V. Thongpool, P. Asanithi, P. Limsuwan, Preparation and characterization of alumina nanoparticles in deionized water using laser ablation technique, J. Nanomater. (2012) 819403, https://doi.org/10.1155/2012/819403.

[11] A. Mukherjee, I. Mohammed Sadiq, T.C. Prathna, N. Chandrasekaran, Science against microbial pathogens: communicating current research and technological advances, in: A. Mendez-Vilas (Ed.), Antimicrobial Activity of Aluminium Oxide Nanoparticles for Potential Clinical Applications, 2011.

[12] E.H.M.A. El-Hussainy, A.M. Hussein, A. Abdel-Aziz, I. El-Mehasseb, Effects of aluminum oxide (Al2O3) nanoparticles on ECG, myocardial inflammatory cytokines, redox state, and connexin 43 and lipid profile in rats: possible cardioprotective effect of gallic acid, Can. J. Physiol. Pharmacol. 94 (8) (2015), https://doi.org/10.1139/cjpp-2015-0446.

[13] K. Ravindhranath, M. Ramamoorty, Nano aluminum oxides as adsorbents in water remediation methods: a review, Rasayan J. Chem. 10 (3) (2017) 716–722, https://doi.org/10.7324/RJC.2017.1031762.

[14] I.H. Karakas, Z. Karcioglu Karakas, M. Ertugrul, Photocatalytic activity of cobalt aluminate nanoparticles synthesized by microwave-assisted combustion method, J. Phys. Chem. Solid. 161 (2022) 110482, https://doi.org/10.1016/j.jpcs.2021.110482.

[15] F. Manteghi, S.H. Kazemi, M. Peyvandipour, A. Asghari, Preparation and application of cobalt oxide nanostructures as electrode materials for electrochemical supercapacitors, RSC Adv. 5 (2015), https://doi.org/10.1039/C5RA09060A, 76485-76463.

[16] J. Mei, T. Liao, G.A. Ayoko, J. Bell, Z. Sun, Cobalt oxide-based nanoarchitectures for electrochemical energy applications, Prog. Mater. Sci. 103 (2019) 596–677, https://doi.org/10.1016/j.pmatsci.2019.03.001.

[17] S.M. Ansari, R.D. Bhor, K.R. Pai, D. Sen, S. Mazumder, K. Ghosh, Y.D. Kolekar, C.V. Ramana, Cobalt nanoparticles for biomedical applications: facile synthesis, physiochemical characterization, cytotoxicity behavior and biocompatibility, Appl. Surf. Sci. 414 (2017) 171–187, https://doi.org/10.1016/j.apsusc.2017.03.002.

[18] V.A. Bautin, A.G. Seferyan, M.S. Nesmeyanov, N.A. Usov, Magnetic properties of polycrystalline cobalt nanoparticles, AIP Adv. 7 (2017) 045103, https://doi.org/10.1063/1.4979889.

[19] A.A. Vodyashkin, P. Kezimana, F.Y. Prokonov, I.A. Vasilenko, Y.M. Stanishevskiy, Current methods for synthesis and potential applications of cobalt nanoparticles: a review, Cryst 12 (2) (2022) 272, https://doi.org/10.3390/cryst12020272.

[20] F. Maldonado, A. Stashans, Al-doped ZnO: electronic, electrical and structural properties, J. Phys. Chem. Solid. 71 (5) (2010) 784–787, https://doi.org/10.1016/j.jpcs.2010.02.001.

[21] P. Raghu, N. Srinatha, C.S. Naveen, H.M. Mahesh, B. Angadi, Investigation on the effect of Al concentration on the structural, optical and electrical properties of spin coated Al:ZnO thin films, J. Alloys Compd. 694 (2017) 68–75, https://doi.org/10.1016/j.jallcom.2016.09.290.

[22] V. Galstyan, E. Comini, C. Baratto, G. Faglia, G. Sberveglieri, Nanostructured ZnO chemical gas sensors, Ceram. Int. 41 (10 Part B) (2015) 14239–14244, https://doi.org/10.1016/j.ceramint.2015.07.052.

[23] S. Devendiran, A.K. Priya, D. Sastikumar, Design of aluminium oxide (Al2O3) fiber optic gas sensor based on detection of refracted light in evanescent mode from the side-polished modified clad region, Sens. Actuators B Chem. 361 (2022) 131738, https://doi.org/10.1016/j.snb.2022.131738.

[24] N. Dey, S. Vickram, S. Thanigaivel, C. Kamatchi, R. Subbaiya, N. Karmegam, M. Govarthanan, Graphene materials: armor against nosocomial infections and biofilm formation – a review, Environ. Res. 214 (2) (2022) 113867, https://doi.org/10.1016/j.envres.2022.113867.

[25] H.A. Khan, A. Ahmad, R. Mehboob, Nosocomial infections and their control strategies, Asian Pac. J. Trop. Biomed. 5 (7) (2015) 509–514, https://doi.org/10.1016/j.apjtb.2015.05.001, 2015.

[26] M. Haque, M. Sartelli, J. McKimm, M.A. Bakar, Health care-associated infections – an overview, Infect. Drug Resist. 11 (2018) 2321–2333, https://doi.org/10.2147/IDR.S177247.

[27] T.M. Uddin, A.J. Chakraborty, A. Khusro, B.R.M. Zidan, S. Mitra, T. Bin Emran, K. Dhama, M.K. Ripon, M. Gajdacs, M.U. Sahibzada, M.J. Hossain, N. Koirala, Antibiotic resistance in microbes: history, mechanisms, therapeutic strategies and future prospects, J. Infect. Public Health 14 (12) (2021) 1750–1766, https://doi.org/10.1016/j.jiph.2021.10.020.

[28] R. Belal, A. Gad, Zinc oxide nanoparticles induce oxidative stress, genotoxicity, and apoptosis in the hemocytes of *Bombyx mori* larvae, Sci. Rep. 13 (2023) 3520, https://doi.org/10.1038/s41598-023-30444-y.

[29] A.L. Barry, M.D.H. Nadler, P.D.L.B. Reller, M.M.S.M.D. Christine C. Sanders, PhD. Jana M. Swenson, M26-A Methods for Determining Bactericidal Activity of Antimicrobial Agents; Approved Guideline This Document Provides Procedures for Determining the Lethal Activity of Antimicrobial Agents, vol. 19, Clinical and Laboratory Standards Institute, 1999.

[30] S.A. Hosseini, Production of γ-Al2O3 from kaolin, Open J. Phys. Chem. 1 (2) (2011) 23–27, https://doi.org/10.4236/ojpc.2011.12004.

[31] N. Srisawad, W. Chaitree, O. Mekasuwandumrong, P. Praserthdam, J. Panpranot, Formation of CoAl2O4 nanoparticles via low-temperature solid-state reaction of fine gibbsite and cobalt precursor, J. Nanomater. 108369 (2012), https://doi.org/10.1155/2012/108369.

[32] E.R. Abaide, C.G. Anchieta, V.S. Foletto, B. Reinehr, L.F. Nunes, R.C. Kuhn, M.A. Mazutti, E.L. Foletto, Production of copper and cobalt aluminate spinels and their application as supports for inulinase immobilization, Mater. Res. 18 (5) (2015) 1062–1069, https://doi.org/10.1590/1516-1439.031415.

[33] V. Saxena, L.M. Pandey, Synthesis, characterization and antibacterial activity of aluminum doped zinc oxide, Mater. Today Proc. 18 (3) (2019) 1388–1400, https://doi.org/10.1016/j.matpr.2019.06.605.

[34] D. Gingasu, I. Mindru, D.C. Culita, G. Marinescu, S. Somacescu, A. Ianculescu, V.A. Surdu, S. Preda, O. Oprea, B.S. Vasile, *Mentha piperita*-mediated synthesis of cobalt aluminate nanoparticles and their photocatalytic activity, J. Mater. Sci. Mater. Electron. 32 (2021) 11220–11231, https://doi.org/10.1007/s10854-021-05791-z.

[35] D. Manyasree, P. Kiranmayi, R.V.D. Ravi Kumar, Synthesis, characterization, and antibacterial activity of aluminum oxide nanoparticles, Int. J. Pharm. Sci. 10 (1) (2018) 32–35, https://doi.org/10.22159/ijpps.2018v10i1.20636.

[36] M.J. Klink, N. Laloo, A. Leudjo Taka, V.E. Pakade, M.E. Monapathi, J.S. Modise, Synthesis, characterization and antimicrobial activity of zinc oxide nanoparticles against selected waterborne bacterial and yeast pathogens, Mol 27 (11) (2022) 3532, https://doi.org/10.3390/molecules27113532.
[37] A. Alkahlout, N. Al Dahoudi, I. Grobelsek, M. Jilavi, P.W. de Oliveira, Synthesis and characterization of aluminum doped zinc oxide nanostructures via hydrothermal route, J. Mater. 2014 (2014) 235638, https://doi.org/10.1155/2014/235638.
[38] N. Ahammed, M.D. Samim Hassan, M. Hassan, Effects of aluminum (Al) incorporation on structural, optical and thermal properties of ZnO nanoparticles, Mater. Sci.-Poland. 36 (3) (2018) 419–426. http://creativecommons.org/licenses/by-nc-nd/4.0/.
[39] A.A. Khassin, V.F. Anufrienko, V.N. Ikorskii, L.M. Plyasova, G.N. Kustova, T.V. Larina, I.Y. Molina, V.N. Parmon, Physico-chemical study on the state of cobalt in a precipitated cobalt-aluminum oxide system, Phys. Chem. Chem. Phys. 4 (2002) 4236–4243, https://doi.org/10.1039/B201967A.
[40] L. Torkian, M. Daghighi, Effects of β-alanine on morphology and optical properties of CoAl 2O4 nanopowders as a blue pigment, Adv. Powder Technol. 25 (2) (2014) 739–744, https://doi.org/10.1016/j.apt.2013.11.003.
[41] T. Gholami, M. Salavati-Niasari, S. Varshoy, Investigation of the electrochemical hydrogen storage and photocatalytic properties of CoAl2O4 pigment: green synthesis and characterization, Int. J. Hydrogen Energy 41 (22) (2016) 9418–9426, https://doi.org/10.1016/j.ijhydene.2016.03.144.
[42] A. Jouya Talaei, N. Zarei, A. Hasan, S. Haj Bloukh, Z. Edis, N. Abbasi Gamasaee, M. Heidarzadeh, M. Babadaei, K. Shahpasand, M. Sharifi, K. Akhatri, S. Khan, M. Xue, M. Falahati, Fabrication of inorganic alumina particles at nanoscale by a pulsed laser ablation technique in liquid and exploring their protein binding, anticancer and antipathogenic activities, Arab. J. Chem. 14 (2) (2021) 102923, https://doi.org/10.1016/j.arabjc.2020.102923.
[43] I. Ahmad, M.Y. Alshahrani, S. Wahab, A.I. Al-Harbi, N. Nisar, Y. Alraey, A. Alqahtani, M.A. Mir, S. Irfan, M. Saeed, Zinc oxide nanoparticle: an effective antibacterial agent against pathogenic bacterial isolates, J. King Saud Univ. Sci. 34 (5) (2022) 102110, https://doi.org/10.1016/j.jksus.2022.102110.
[44] J. Pasquet, Y. Chevalier, J. Elletier, E. Couval, D. Bouvier, M.A. Bolzinger, The contribution of zinc ions to the antimicrobial activity of zinc oxide, Colloids Surf. A: Physicochem. Eng. Asp. 457 (2014) 263–274, https://doi.org/10.1016/j.colsurfa.2014.05.057.
[45] P.M. Baumert, J. Camp, M. Goiz, S. Schuster, W.V. Kern, A. Mischnik, Detection of high-level rifaximin resistance in enteric bacteria by agar screen, Microb. Drug Resist. 26 (2020) 6, https://doi.org/10.1089/mdr.2019.0295.
[46] B. El Shazely, G. Yu, P.R. Johnston, J. Rolff, Resistance evolution against antimicrobial peptides in *Staphylococcus aureus* alters pharmacodynamics beyond the MIC, Front. Microbiol. 11 (2020) 103, https://doi.org/10.3389/fmicb.2020.00103.
[47] T.S. Sihotang, A.D. Widodo, P.D. Endraswari, Effect of Ciprofloxacin, Levofloxacin, and Ofloxacin on *Pseudomonas aeruginosa:* a case control study with time kill curve analysis, Ann. Med. Surg. 82 (2022) 104674, https://doi.org/10.1016/j.amsu.2022.104674.
[48] M. Balouiri, M. Sadiki, S.K. Ibnsouda, Methods for in vitro evaluating antimicrobial activity: a review, J. Pharm. Anal. 6 (2) (2016) 71–79, https://doi.org/10.1016/j.jpha.2015.11.005.
[49] A. Sirelkhatim, S. Mahmud, A. Seeni, N.H.M. Kaus, L.C. Ann, S.K.M. Bakhori, H. Hasan, D. Mohamad, Review on zinc oxide nanoparticles: antibacterial activity and toxicity mechanism, Nano-Micro Lett. 7 (3) (2015) 219–242, https://doi.org/10.1007/s40820-015-0040-x.
[50] S.X.T. Liang, L.S. Wong, Y.M. Lim, P.F. Lee, S. Djearamane, Effects of zinc oxide nanoparticles on Streptococcus pyogenes, S. Afr. J. Chem. Eng. 34 (2020) 63–71. https://hdl.handle.net/10520/EJC-1fca662d8b.
[51] L. Wang, C. Hu, L. Shao, The antimicrobial activity of nanoparticles: present situation and prospects for the future, Int. J. Nanomed. 12 (2017) 1227–1249, https://doi.org/10.2147/IJN.S121956.